Probing the Molecular Level of Polyimide-Based Solvent Resistant Nanofiltration Membranes with Positron Annihilation Spectroscopy

Angels Cano-Odena,[†] Pieter Vandezande,[†,‡] Katrien Hendrix,[†] Rolph Zaman,[†] Khaled Mostafa,[§] Werner Egger,[||] Peter Sperr,[||] Jérémie De Baerdemaeker,[§,⊥] and Ivo F. J. Vankelecom*[,†]

Centre for Surface Chemistry and Catalysis, Faculty of Bioscience Engineering, Katholieke Universiteit Leuven, Kasteelpark Arenberg 23—box 2461, B-3001 Leuven, Belgium, NUMAT (Nuclear Methods in Materials Science), Department of Subatomic and Radiation Physics, Ghent University, Proeftuinstraat 86, B-9000 Gent, Belgium, and LRT2, Werner-Heisenberg-Weg39, Universität der Bundeswehr München, D-85577 Neubiberg, Germany

Received: February 11, 2009; Revised Manuscript Received: May 28, 2009

Positron annihilation spectroscopy (PAS) has been performed to link fundamental polymer properties to membrane performance, more specifically for polyimide (PI)-based solvent-resistant nanofiltration membranes. Laboratory-made membranes with well-known properties were applied first to define proper pretreatment conditions for the membrane to allow PAS-analysis and to allow more correct linking of PAS results to membrane properties. This knowledge was then applied to probe the structure of commercial PI-based Starmem membranes.

1. Introduction

The need for cleaner and more energy efficient technologies, together with increased concerns about the environment and other socioeconomical impulses, has enhanced the interest in solvent resistant nanofiltration (SRNF) as a viable sustainable alternative for energy consuming and waste generating separation techniques, such as distillation and crystallization or extraction in food,[1] chemical,[2] petrochemical,[3,4] pharmaceutical,[5] and semiconductor industries.[6] Depending on the definition, SRNF-membranes show molecular weight cutoff values between 200 and 1000 Da when applying a pressure gradient over the membrane of >5 bar. SRNF allows separations at a molecular level, e.g. separating organic solutes such as catalysts or extracted fats from their solvents.[7]

In general, knowing the correct structure of a membrane is essential to interpret correctly filtration results and deliver the right input to transport models. Accurate structural knowledge also allows better prediction utility of a certain membrane for a given separation problem. Getting such structural information about the selective top-layer of SRNF-membranes is extremely difficult. First of all, the top-layers are thin: in the micrometer-range for solvent-cast membranes and in the nanometer-range for membranes prepared via phase inversion. Second, being capable of separating on a molecular level, the pores (or, depending on the context, free volume elements) in SRNF-membranes are not larger than a few angstroms, hence requiring a very high spatial resolution of the analytical technique. Third, the majority of the SRNF-membranes is polymeric in nature, such as, for instance, polyimide (PI), polyethersulfone (PES), polyacrylonitrile (PAN), and poly(vinylidene) fluoride (PVDF), thus easily creating artifacts and distortions during sample preparation. Probing the porosity of an SRNF-membrane is thus far from trivial; it is not possible with common techniques, such as nitrogen adsorption or SEM, and it is even very hard with TEM or AFM.

Positron annihilation spectroscopy (PAS) is a relatively new technique that has been used to probe structures at an atomic scale in semiconductors, metals, dielectrics, clays, and polymers. It is based on the interaction of the electrons in these media with positrons. It is a mild, nondestructive method that can be applied to samples under ambient conditions.[8] In membrane technology, PAS has already been applied in the characterization of commercial pervaporation[9] and gas separation membranes.[10,11] It has also been recently used to study the free-volume depth profile of commercial nanofiltration membranes for aqueous applications.[12,13] Recent studies have also been performed to evaluate structural changes and free volume properties in thin film polyamide (PA)-PAN pervaporation membranes prepared by interfacial polymerization.[14] Nevertheless, no clear correlation was found between the PAS data and the flux and selectivity in the pervaporation separation of 2-propanol aqueous solutions. From lifetime measurements, the effect of the concentration of the amine monomer in the synthesis of the selective PA top layer in the free volume could be related to the selectivity of these membranes.[15] An in-depth study of the process and the parameters involved in the membrane synthesis via phase inversion has not been carried out so far. (Solvent induced) phase inversion is a very popular membrane synthesis technique in which a cast polymer solution is solidified by immersion in a nonsolvent bath. During the solidification, an asymmetric pore structure is often formed, with the smallest pores on top and the widest below. Such asymmetric structure is ideal for SRNF-membranes, where the skin determines the separation and the bottom structure gives mechanical support. Moreover, a need to link information provided by PAS to membrane performance is clearly still needed for a better understanding of separation processes.

Most PAS applications study the lifetime of *ortho*-positroniums (*o*-PSs).[16] An *o*-PS is a metastable bound state consisting on an electron and a positron. It resides mostly in free volume

* Corresponding author. Telephone: +32-16-321594. Fax: +32-16-321998. E-mail: ivo.vankelecom@biw.kuleuven.be.
† Katholieke Universiteit Leuven.
‡ Present address: Flemish Institute for Technological Research (VITO), Boeretang 200, B-2400 Mol, Belgium.
§ Ghent University.
|| Universität der Bundeswehr München.
⊥ Present address: NV Bekaert SA, Bekaertstraat 2, B-8550 Zwevegem, Belgium.

10.1021/jp9012653 CCC: $40.75
Published on Web 07/02/2009

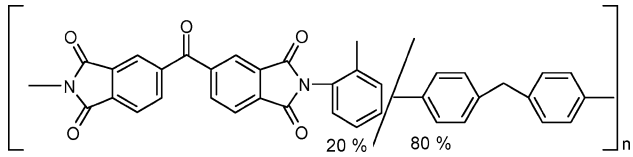

Figure 1. Chemical structure of Lenzing P84 PI.

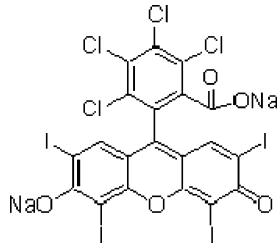

Figure 2. Chemical structure of Rose Bengal.

elements, where the electronic density of the material is lower and therefore the probability of the positron to annihilate with electrons of the surroundings is also lower. The lifetime of such species can be related to cavity sizes and their distribution (see also the Experimental Section). Using commercial membranes with only vaguely defined structure and composition does not allow verification of the obtained PAS data with the actual membrane physicochemical properties and thus limits interpretation of membrane performance. Moreover, different chemical compositions influence PAS results (via the S parameter) and simply do not allow comparison among different membrane materials. It is the purpose of this paper to verify PAS data with anticipated membrane properties and to try to define trends that can be qualitatively expected from basic phase inversion chemistry. A systematic study of the effect of synthesis parameters involved in the phase inversion process will be linked to membrane performance and a structural characterization at the molecular level via PAS. One of the best SRNF-materials, a polyimide-based (PI) membrane, was selected for this study. PI has good film forming properties to enable membrane fabrication, and it is cheap and commercially available. In addition, cross-linking reaction with diamines has been reported as a successful method to enhance the chemical stability of the polymer toward polar aprotic solvents,[17,18] which are common solvents for PI. Previous studies of PI with positron techniques have been carried out mainly by doing lifetime measurements to correlate with free volume sizes and diffusion coefficients in gas separation membranes.[19] This will be the first time that PAS will be applied in the study of SRNF membranes.

2. Materials and Methods

2.1. Chemicals. Lenzing P84 PI (Figure 1), a copolymer of 20% 3,3′,4,4′-benzophenone tetracarboxylic dianhydride and methylphenylenediamine and 80% toluenediamine, was kindly supplied by Evonik, as a 25 wt % solution in *N*-methylpyrrolidinone (NMP) (Inspec Fibers GmbH, Austria). Tetrahydrofuran (THF, Acros) and NMP (Acros) were used as solvents to prepare casting solutions. Isopropyl alcohol (IPA, VWR), toluene (Acros), 2-methyl-4-pentanone (MIBK, Acros), and mineral oil (P3, Pfeiffer) were used to condition the membranes. IPA was selected as solvent in the filtration experiments, while Rose Bengal (RB, 1017 Da, Fluka) was used as solute (Figure 2). All solvents were analytical grade and used without any further purification or treatment. Commercial PI-based SRNF membranes, i.e. Starmem 120, 220, and 240, with nominal molecular weight cutoff (MWCO) values of 200, 280, and 400 g/mol, respectively (based on 90% rejection of normal alkanes in toluene), were purchased from Membrane Extraction Technology Ltd. (U.K.).

TABLE 1: Synthesis Parameters of PI-Based SRNF Membranes: Composition of Dope Solutions and Evaporation Times

	composition dope solution (wt %)			
membrane	PI	NMP	THF	evaporation time (s)
N1	14.00	71.67	14.33	30
N2	16.50	69.58	13.92	30
N3	19.00	67.50	13.50	30
N4	21.50	65.42	13.08	30

2.2. Preparation of Integrally Skinned Asymmetric PI-Based SRNF Membranes. Asymmetric PI membranes were prepared from Lenzing P84 PI, which was dissolved with NMP and THF. After magnetic stirring overnight, the PI dope solutions were cast (1.2 m/min) at room temperature as 250 μm thick films on an NMP-saturated Novatexx 2471 polypropylene/polyethylene nonwoven textile, kindly supplied by Freudenberg (Germany), using a custom-designed casting box and an automatic film applicator (Elcometer, Belgium). The nascent films were then shortly (30−600 s) exposed to ambient air to allow partial evaporation of the volatile THF from the surface, after which the films were immersed into a water bath at room temperature to induce membrane solidification. A series of membranes varying the PI concentration (N1−N4) was manufactured (Table 1). The NMP:THF weight ratio of the added solvents was invariably maintained at 5:1.

In order to avoid pore collapse upon drying and enhance the performance of the membranes, a sequential solvent exchange procedure combined with mineral oil impregnation was carried out.[20] The treatment involved immersion of the membranes in IPA for 3 h and subsequently for 3 days in a toluene/MIBK/oil bath with a 40/40/20 volumetric composition. The excess liquid was carefully wiped off with tissue paper, after which the membranes were dried for 1 h at 60 °C and stored in a dry state.

Membrane samples for PAS and SEM measurements were post-treated differently, since the presence of mineral oil in the pores would interfere with the vacuum conditions. These samples were therefore transferred from the coagulation bath to IPA (3 h) and subsequently to a hexane/IPA (50/50 vol/vol %) bath (3 days), and then dried at room temperature (1 h).

2.3. Filtration Experiments. The separation performance of the asymmetric PI membranes in SRNF was assessed through filtration experiments at room temperature. Circular coupons were cut from the PI membrane sheets, mounted in a laboratory-made stainless steel dead-end pressure cell with an active filtration area of 12.56 cm^2, and sealed with Kalrez O-rings. A 35 μM solution of RB (1017 Da) in IPA was used as feed (Figure 2). 50 mL of feed solution was poured into the cell, stirred at 700 rpm, and pressurized with nitrogen gas at 4 bar. Commercial PI-based Starmem 120, 220, and 240 membranes were tested as a reference (MWCO values, provided by the manufacturer, are 200, 280, and 400 Da, respectively). Permeate samples were collected in closed flasks, weighed, and analyzed to determine permeabilities ($L \cdot m^{-2} \cdot h^{-1} \cdot bar^{-1}$) and selectivities. To avoid initial nonequilibrium conditions and wash out the mineral oil conditioner, the initial filtrate was discarded, and collection of permeate sample was only started after 45 min of filtration. Rejections (%) are defined as $(1 - C_p/C_f) \times 100$, where C_f and C_p denote the solute concentration in the initial feed and in the permeate, respectively. Dye concentrations were

analyzed on a Perkin-Elmer Lamda 12 UV−vis spectrophotometer at 555 nm. Filtrations were performed in duplicate. Average performances are shown.

2.4. Scanning Electronic Microspcopy. SEM pictures of membrane cross sections were acquired on a Philips XL 30 FEG scanning electron microscope, a semi-in-lens type microscope equipped with a cold field-emission electron source. Cross sections were obtained by breaking dry membranes, post-treated as discussed in section 2.2, under liquid nitrogen. Samples were then mounted onto SEM sample holders and coated with a 1.5−2 nm thick gold layer to reduce sample charging under the electron beam, using a Cressington HR208 (UK) high resolution sputter coater.

2.5. Positron Annihilation Spectroscopy (PAS). Positrons, the antiparticles of electrons, are emitted from the β^+-decay of radioactive isotopes.[21] They exhibit an energy distribution up to 540 KeV and can penetrate deep into a sample. Nevertheless, most of the studies in materials are focused on the structure and defects near the surface. The so-called slow positron beam techniques require only a fraction of low energy monoenergetic slow positrons to achieve a small penetration depth, by using different moderation processes to adjust the positron energy in a range of low energy around a few eletronvolts.[22] Differences in distribution, concentration, and pore sizes at different depths in membranes can be estimated from the energy of annihilation. The use of a variable low energy positron beam enables the study of the characteristic annihilation of the positronium from the surface down to a few micrometers.

Positrons diffuse in a material and annihilate with an electron of the sample into γ-rays. In free volumes, where the electron density is low, a fraction of these positrons can form with an electron a metastable bound state called positronium (Ps), with two possible states: *para*-Ps (p-Ps), with antiparallel spins, or *ortho*-Ps (*o*-Ps), with parallel spins, in a ratio 1:3. *p*-Ps annihilates intrinsically mainly into two γ-rays of 511 keV with an annihilation lifetime in vacuum of 0.125 ns (comparable to free positrons). *o*-Ps has a longer lifetime (142.08 ns) to interact with surroundings. Therefore, it either annihilates in vacuum into three γ-rays to conserve spin (self-annihilation) or annihilates with electrons in the surrounding matter (pick-off annihilation), resulting in two γ-rays. The Compton to peak (R) parameter is defined as the ratio between $3\gamma/2\gamma$ emissions. The profile of the R parameter as a function of the energy of irradiation provides information about the relative size and concentration of pores. The so-called S parameter measures the Doppler broadening of the annihilation peak at 511 keV, which depends on the momentum distribution of the electrons at the site of annihilation. The S parameter is expressed as the ratio of the counts in a certain window compared to the number of counts at the energy of the 511 keV peak. In defects, the fraction of valence electrons (with lower momentum) taking part in the annihilation process increases compared with that of the core electrons. An increase of positrons entrapped in such free volumes increases the S parameter. It is related to the chemistry of the material and sensitive to structural changes and defects and their concentration.

Positron annihilation lifetime spectroscopy (PALS) provides information from the differences in the lifetime of *o*-Ps before annihilation, which is related to the free volume cavities radius (r_i), according to the Tao−Eldrup equation (eq 1).[23,24] In this equation, pores are considered as spherical cavities with a radius r_i and *o*-Ps is trapped in a spherical region of potential radius $r_o = r + \Delta r$, where Δr is an electron layer of thickness 0.166 nm.

$$T_3 = 0.5\left[1 - \frac{r_i}{r_i + \delta r} + \frac{1}{2\pi}\sin\left(\frac{2\pi r_i}{r_i + \delta r}\right)\right]^{-1} \quad (1)$$

Variable low energy positron experiments were performed both at the Department of Subatomic and Radiation Physics of Ghent University Belgium and at the new NEPOMUC facility of the FRMII research reactor in Garching Germany, while the R parameter and Doppler Broadening experiments were performed at Ghent University. The positron lifetime measurements were performed at the FRMII research center.

The positron beam at Ghent University is described elsewhere.[25] A magnetically guided continuous low energy positron beam from a moderated 22Na source can be accelerated and implanted into the samples with energies ranging from a few electronvolts up to 30 keV, corresponding in polymers to an implantation depth of maximum 10 μm. The annihilation radiation detected by a high purity Ge detector (resolution fwhm 1.2 keV at 511 keV) is parametrized into the R and S parameters.

The positron beamline used at the NEPOMUC[26] slow positron facility at the FRMII is the pulsed low energy positron system PLEPS. The continuous low energy positron beam from the neutron reactor, with an intensity of approximately 10^9 low energy positrons per second is modulated at 50 MHz into a pulse of approximately 250 ps.The lifetime spectra were decomposed using LT9 software.[27] For each of the samples, the evolution of the R parameter profile measured at the Ghent University was used to determine the energy selection to perform the lifetime experiments at FRMII.

3. Results and Discussion

3.1. Influence of the Post-treatment on Membrane Performance. In order to acquire positron signals, an adapted membrane preconditioning was needed. The oil, present in the pores as a consequence of the conventional sequential solvent exchange described in section 2.2, was found to quench the signal and had to be removed. Also, some commercial Starmem membranes had a similar problem. The addition of oil is commonly used to prevent pore collapse during the drying step.[28] It also improves the membrane handling by making the membranes more flexible.

It was first investigated to what extent such changed membrane conditioning influenced membrane performance. Table 2 shows that an alternative solvent exchange in IPA/hexane, and thus without any oil present, roughly halves permeabilities compared to the standard post-treatment with MIBK/toluene/oil.[29,30]

Some of the lab-made samples had undergone the oil conditioning already before realizing this problem. Also, the Starmem membranes were delivered in a conditioned state. In

TABLE 2: Retention and Permeabilities after Different Solvent Exchange Post-treatments[a]

membrane	solute/solvent	retention (%)	permeability ($L \cdot m^{-2} \cdot h^{-1} \cdot bar^{-1}$)
N5 (oil)	RB/IPA	77 ± 3	10 ± 2
N5 IPA/hexane	RB/IPA	78 ± 3	4.7 ± 0.4
N5 rev(oil;hex)	RB/IPA	62 ± 5	5 ± 1

[a] Oil: conventional (MIBK/toluene/oil) treatment. IPA/hexane after immersion in IPA for 3 h, membrane transfer to (IPA/hexane) (50/50). Rev(oil;hex) post-treatment by immersion in (MIBK/toluene/oil), followed by flushing with IPA, and membrane transfer to (IPA/hexane) (50/50). Results are an average of three replicates with different membrane coupons.

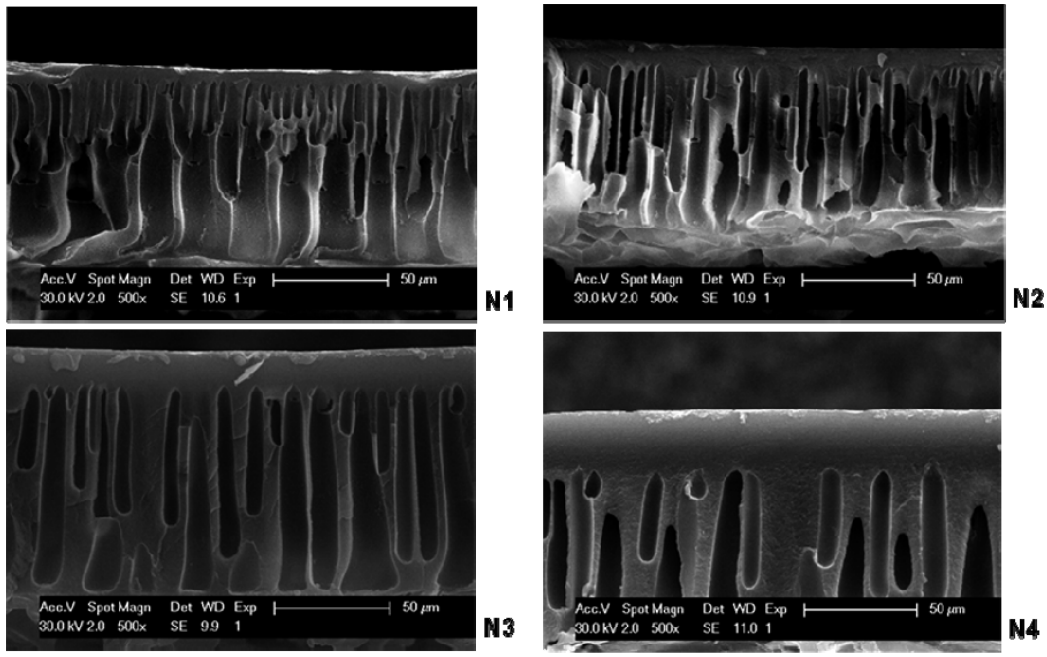

Figure 3. SEM cross sections of P84-based asymmetric membranes prepared from casting solutions with different polymer content.

order to allow PAS on these samples anyhow, oil thus had to be removed first and it was studied how such treatment changed the performance. A lab-made membrane was thus tested without oil treatment, with oil treatment, and with a "rinsed back" treatment in which the impregnated oil was flushed out during a preliminary IPA-filtration at 20 bar during 1 h. As this membrane showed the same permeability as the membrane that had never been contacted with oil (N5 IPA/hex), the oil post-treatment is clearly reversible.

Removal of the oil thus decreases the membrane permeability, but the reversibility of the treatment proves that it does not change anything intrinsic to the membrane morphology. Even though not probing the exact "real time" membrane properties during filtration, PAS will thus clearly allow comparison of membrane properties.

3.2. Effect of Polymer Concentration. It is known that a higher polymer concentration in the casting solution makes the nonsolvent diffuse more slowly into the polymer dope during phase inversion, thus slowing down precipitation of the polymer and creating thicker and denser skin layers with lower porosities.[31,32] SEM cross sections of membranes differing in polymer concentration in the casting solution confirm this trend (Figure 3).

SEM images show that the thickness of the skin layer of the membranes increases with higher polymer concentrations, reflected in an important effect in membrane performance shown in Table 3. As expected, an increased P84 polymer concentration in the casting solution improves RB retention at the expense of permeability. Membranes with lower polymer concentrations show extremely high permeabilities but retain RB insufficiently. The highest RB retention in IPA is achieved with the densest membrane (N4). Although it did not reach the retention of commercial membranes yet, it showed a remarkable 20-fold higher permeability with respect to them.

From the SEM images, two main regions can be differentiated in membrane cross sections. These regions will be referred to in this paper as skin and bulk layers (Figure 4a). In PAS, the evolution of the *R* parameter with respect to the energy of irradiation gives an indication of the relative porosity as a

TABLE 3: Retention of RB and Permeabilities for Different PI-Membranes in Different Solvents[a]

membrane	solute/solvent	retention (%)	permeability ($L \cdot m^{-2} \cdot h^{-1} \cdot bar^{-1}$)
N1	RB/IPA	63 ± 22	191 ± 7
N2	RB/IPA	63 ± 2	69 ± 5
N3	RB/IPA	61 ± 3	11.2 ± 0.2
N4	RB/IPA	87 ± 3	14.6 ± 0.6
Starmem 120	RB/IPA	99.8 ± 0.1	0.81 ± 0.01
Starmem 228	RB/IPA	91 ± 7	0.127 ± 0.001
Starmem 240	RB/IPA	98 ± 2	0.52 ± 0.01

[a] Results are an average of three replicates taken from different membrane coupons.

function of depth in a membrane cross section (Figure 4b). For comparison and to rule out any influence on the measurement geometry, the *R* parameter data was normalized; therefore, its analysis can only be used to interpret the porosity depth evolution and to define the energy to measure lifetime. Compared to SEM, this technique only covers a much thinner range of a few micrometers in the skin layer (see second *x*-axis in Figure 4b). Even in such a small region, PAS still allows us to distinguish several subregions. These will be defined in this paper as "surface layer", "intermediate layer", and "sublayer", respectively, as a function of increasing depth. Previous PAS studies on modified PAN membranes with interfacial polymerized polyamide layers on top of modified PAN also reported the existence of a multilayer structure (so-called dense, transition, and porous layers in a PAN-membrane cross section).[14] In the present case, we thus distinguish an extra layer, since our sublayer (visible in PAS only; in SEM, it still appears as fully dense) is thus still distinguished from the bulk layer (visible in SEM only (being localized too deep for PAS-observation; see second axis in Figure 4b) and characterized by the presence of macrovoids). In the earlier work, only one layer was defined below the transition layer.

At low implantation energies (around 2 keV), *R* values are low, as an indication of a low porosity of the surface layer. As the energy of implantation increases, entering thus deeper in the material, the increasing *R* reflects an increasing porosity.

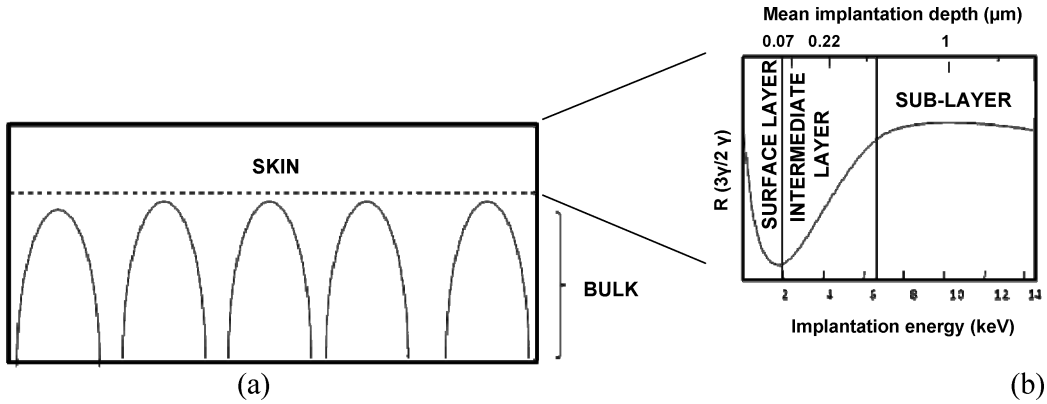

Figure 4. Representation of the different regions in the membrane cross section that can be studied with SEM (a) and PAS (b).

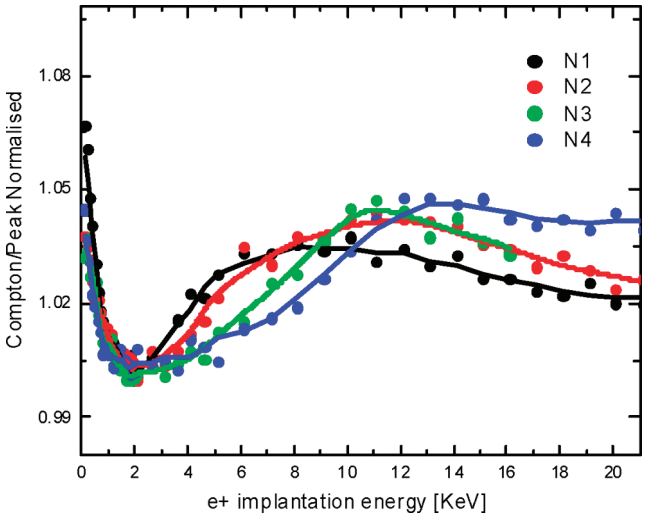

Figure 5. Evolution *R* parameter of P84-based membranes with different polymer content.

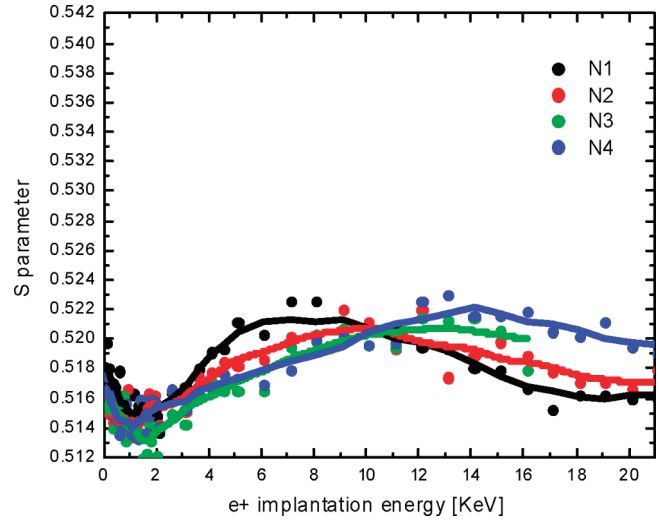

Figure 6. Evolution of *S* parameter P84-based membranes with different polymer content in the precursor solution.

From this evolution of *R* as a function of the energy, it is thus possible to compare the thicknesses of surface, intermediate, and sublayers between different samples. It also gives an indication of the evolution from the skin layer to the porous sublayer. Figure 5 represents the data of membranes N1−N4. *R* has very high values near the surface, because a large fraction of the implanted positrons diffuses back to the surface, forms positronium, and self-annihilates outside of the sample in the vacuum, leading to a high 3γ-value. The initial part at energies far below 2 keV indicates the decreasing fraction of positrons that still reach the surface. As the energy of implantation increases further, the positron can enter deeper in the material and reach the point where no surface signature is visible anymore. *R* is low in this region, indicating that the porosity of the material is low there. From ±3 keV onward, the increase of *R* indicates an increase of the fraction of self-annihilating positroniums, phenomena that mostly take place in bigger pores or free volume elements. This thus implies that an intermediate layer with steadily increasing porosity exists, right below the dense surface layer. At still higher implantation energies, the *R* parameter reaches an almost constant value, which corresponds to the more porous membrane sublayer. Still deeper in the membrane—not being probed by PAS anymore—the even higher porosity of the SEM-observable bulk layer exists.

Comparing the PAS profiles of membranes prepared from casting solutions with different polymer content shows that an increased polymer concentration leads to an increased thickness of the low porosity surface layer, as the lowest *R* values are found at higher energies of implantation (thus deeper). Also, the evolution between the minimal *R*-value in the surface layer and the higher *R*-values of the sublayer is steeper for the membranes with lower PI-content, indicating a more abrupt change between the low porosities of the skin and the higher porosity of the sublayer. When the polymer concentration increases, the evolution is more gradual (lower slope of the curve in Figure 5). This thus means that low membrane permeabilities coincide with a lower *R* parameter (less porosity) in the surface and a more gradual transition to the wider pores of the sublayer.

TABLE 4: *o*-Ps Intensities and Lifetime for P84-Based Laboratory-Made Membranes

membrane	$\tau 3$ (ns)	I3	$\tau 4$ (ns)	I4	mean τ (ns)
N1	1.3 ± 0.5	0.4 ± 0.3	38.7 ± 9.9	1.1 ± 0.2	28
N3	0.9 ± 0.1	1.7 ± 0.7	17.6 ± 1.4	1.0 ± 0.1	7.2
N4	1.2 ± 0.2	0.9 ± 0.3	21.4 ± 5.5	0.4 ± 0.1	8

With an identical chemical composition for membranes N1−N4, the *S* parameter can be used too. The evolution of this parameter (Figure 6) gives similar information in agreement with that obtained from the *R* parameter. In the surface layer, the *S* parameter is not drastically different for the four membranes. In the deeper membrane layers, an increased porosity may again be observed with a clear difference between the four membranes: the porosity in the intermediate layer increases in the order N1 > N2 > N3 > N4.

The *R*-value gives more qualitative information on the depth evolution, but the positron lifetime gives the real quantification

TABLE 5: *o*-Ps Intensities and Lifetime for Starmem Commercial Membranes

membrane	τ3 (ns)	I3	τ4 (ns)	I4	mean τ (ns)
Starmem 120	1.31 ± 0.10	1.03 ± 0.13	30 ± 3	1.26 ± 0.07	17.13
Starmem 228	2.42 ± 0.06	0.46 ± 0.01	0 ± 0	0 ± 0	2.41
Starmem 240	1.15 ± 0.07	1.5 ± 0.18	27.7 ± 1.6	0.4 ± 0.05	14.83

of the positronium analysis. Lifetime measurements at 2 keV, corresponding to a penetration depth of 70 nm, permitted us to determine pore sizes very accurately in the surface layer. Results are shown in Table 4. The intensity of the shortest *o*-Ps lifetime (τ3), representing the smaller free volume sites, is the smallest for N1. The value for the free volume sites of N1 is clearly much larger compared to the cases of N3 and N4. This results in a mean free volume size which is clearly bigger for N1 (*o*-Ps mean lifetimes for N1, 28 ns, for N3, 7.2 ns, and for N4, 8 ns) which can be related to a higher permeability and a lower retention. In view of the results, it seems that a higher retention can be related to a higher ratio between the intensity for the small free volumes (I3) compared to that of the total free volume intensity (I3 + I4), which are 26%, 63%, and 69% for N1, N3, and N4, respectively.

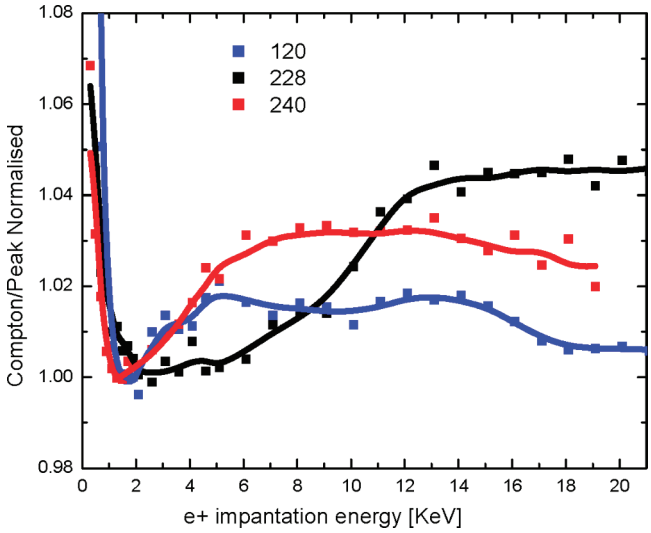

Figure 7. Evolution of the *R* parameters of Starmem 120, 228, and 240 commercial membranes.

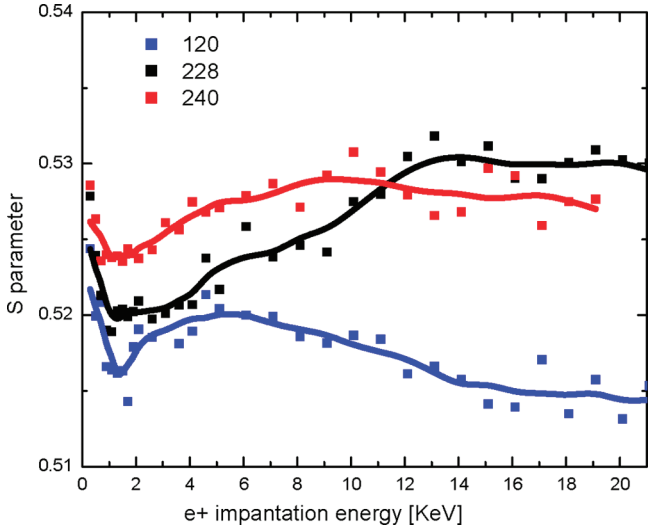

Figure 8. Evolution of the *S* parameters of Starmem 120, 228, and 240 commercial membranes.

In conclusion, membrane performance seems to be determined by the porosity in the surface and intermediate layer found in PAS. PAS thus offers an explanation at the angstrom scale for the macroscopically observed trends. In the surface layer, more pores are present in the more permeable membranes. These pores are also bigger than those in the less permeable membranes.

3.3. Commercial PI-Based Membranes. Commercial Starmem membranes are considered as PI-based SRNF-membranes, but no details about the exact chemical composition are provided. The conditioning agent had to be removed (see above) from the membranes before any PAS-signal could be obtained. Since Matrimid (Huntsman) or Kapton (DuPont) based polyimides do not allow collection of PAS data at all, due to the inhibition of the formation of positroniums, the detection of positron annhilation phenomena would be an indication that the Starmem membranes may contain Lenzing P84 material or the like in their composition.

The RB-retentions of the commercial membranes in filtration experiments (at 50 bar and room temperature) are in general better than the ones of the lab-made membranes, which is in line with the low MWCO-values of the Starmem membranes. The permeability of Starmem 228 is the lowest. This is in line with the evolution of the *R* parameter in PAS measurements (Figure 7). The intermediate layer extends much further in Starmem 228.

The *S* parameter (Figure 8) gives a quite different profile for the three membranes. As the *S* parameter is influenced by the chemical nature of the polymer, it is here however impossible to draw a conclusion with certainty due to the lack of information about the exact chemical composition of the membranes.

PALS measurements in the surface region (2 keV) show that, for Starmem 228, only one *o*-Ps lifetime (τ3) of 2.42 ns can be detected, corresponding to free volumes with a radius of 0.32 nm. The other Starmem membranes have two different *o*-Ps lifetimes: a relatively short one around 1.2 ns (τ3) and a long one around 30 ns (τ4) corresponding to free volume radii of 0.19 and 1 nm, respectively. The mean lifetimes correspond again well with the relative differences in permeability. As for the laboratory-made membranes, the retention would be related to the ratio of the intensity of the small free volume sites to the larger ones. Nevertheless, unequivocal conclusions cannot be drawn because although Starmem228 seems only to have small free volume sites, these are >50% bigger in radius (longer τ3) than those for the other two Stamem. In any case, since these measurements are carried out in the surface layer, they again confirm the role of this layer in the permeability of these commercial membranes.

4. Conclusions

PA(L)S clearly has the potential to add a level of understanding to the current knowledge about (mostly SEM-obtained) the structure of SRNF membranes and its link with filtration performance. PAS probes membrane porosities down to a molecular level, as exemplified here for PI-based SRNF-membranes prepared via phase-inversion. Studies on lab-made membranes with known performance and composition allowed

us to interpret more correctly PA(L)S data than literature studies applied on less known commercial membranes. First of all, a correct membrane pretreatment was found to be essential to enable PA(L)S measurements.

In a set of membranes in which the polymer concentration in the casting solution was increased, SEM pictures showed increasing skin layers to explain decreasing permeabilities. Whereas this was the end point of most earlier studies, the PA(L)S data revealed extra information, as the SEM skin layers were found to consist on their turn of three different regions: a surface layer with low porosity, a transition layer with steadily increasing porosity, and a more porous sublayer. The porosity of the first two layers could be correlated with membrane permeabilities. Lifetime measurements added to the interpretation that a low porosity in the surface layer was in this case due to both a decreased number of pores and a smaller amount of pores.

This knowledge was then applied to commercial membranes where unknown chemical compositions make the interpretation of PAL(S) parameters partly impossible. Low porosities could be linked again to the properties of the transition layer and the lifetime measurements in the surface layer.

Acknowledgment. A.C.-O. acknowledges the financial support from the Departament d'Universitats, Recerca i Societat de la Informació (DURSI) from Generalitat de Catalunya for the postdoctoral scholarship (ref 2006 BP-A 10012). The research performed at the FRMII has been supported by the European Commission under the sixth Framework Programme through the Key Action: Strengthening the European Research Area, Research Infrastructures (Contract No. RII3-CT-2003-505925). This research was done in the framework of an I.A.P.-PAI grant (IAP 6/27) sponsored by the Belgian Federal Government and of a GOA grant from K.U.Leuven. I.F.J.V., A.C.-O., K.H., and R.Z. acknowledge the long term structural funding—Methusalem funding by the Flemish Government.

References and Notes

(1) Bargeman, G.; Timmer, M.; van der Horst, C. In *Nanofiltration. Principles and Applications*; Schäfer, A. I., Fane, A. G., White, T. D., Eds.; Elsevier: Oxford, 2005; Chapter 12, pp 305−328.

(2) Rissom, S.; Beliczey, J.; Giffels, G.; Kragl, U.; Wandrey, C. *Tetrahedron: Asymmetry* **1999**, *10*, 923.

(3) White, L. S. *J. Membr. Sci.* **2006**, *286*, 26.

(4) US Patent 7 048 846, 2006.

(5) Shi, D.; Kong, Y.; Yu, J.; Wang, Y.; Yang, J. *Desalination* **2006**, *191*, 309.

(6) Zhang, H.; Wu, A.; Wei, J.; Buschjost, R. Effect of nanofiltration on photochemical integrity; Proceedings of SPIE; 2008; p 6923.

(7) Vandezande, P.; Gevers, L. E. M.; Vankelecom, I. F. J. *Chem. Soc. Rev.* **2008**, *37*, 365.

(8) Goworek, J.; Wawryszczuk, J.; Zaleski, R. *J. Colloid Interface Sci.* **2001**, *243*, 427–432.

(9) Staynarayana, S. V.; Subrahmanyam, V. S.; Verma, H. C.; Sharma, A.; Bhattacharya, P. K. *Polymer* **2006**, *47*, 1300–1307.

(10) Hu, C.-C.; Lee, K.-R.; Ruaan, R.-C.; Jean, Y. C.; Lai, J.-Y. *J. Membr. Sci.* **2006**, *274* (1−2), 192–199.

(11) Merkel, T. C.; Freeman, B. D.; Spontak, R. J.; He, Z.; Pinnau, I.; Meakin, P.; Hill, A. J. *Science* **2002**, *296*, 519–522.

(12) Boussu, K.; Dauwe, C.; Weber, M.; Lynn, K. G.; Depla, D.; Aldea, S.; Vankelecom, I. F. J.; Vandecasteele, C.; Van der Bruggen, B. *ChemPhysChem* **2007**, *8*, 370–379.

(13) De Baerdemaeker, J. *Phys. Status Solidi* **2007**, *4*, 3804–3809.

(14) Chen, H.; Hung, W.-S.; Lo, C.-H.; Huang, S.-H.; Cheng, M.-L.; Liu, G.; Lee, K.-R.; Lai, J.-Y.; Sun, Y.-M.; Hu, C.-C.; Suzuki, R.; Ohdaira, T.; Oshima, N.; Jean, Y. C. *Macromolecules* **2007**, *40*, 7542.

(15) Kim, H. S.; Kwak, S.-Y.; Suzuki, T. *Environ. Sci. Technol.* **2005**, *39*, 1764–1770.

(16) Yin, H. H.; Zejie, Y.; Weitao, M.; Daming, Z. *Plasma Sci. Technol.* **2005**, *7*, 3062–3064.

(17) Vanherck, K.; Vandezande, P.; Aldea, S. O.; Vankelecom, I. F.J. *J. Membr. Sci.* **2008**, *320*, 468–476.

(18) See Toh, Y. H.; Lim, F. W.; Livingston, A. G. *J. Membr. Sci.* **2007**, *301*, 3–10.

(19) Cornelius, C. J.; Marand, E.; Meakin, P.; Hill, A. J.; Freeman, B. D.; Spontak, R. J.; He, Z.; Pinnau, I.; Meakin, P.; Hill, A. J. *Science* **2002**, *296*, 519–522.

(20) Vandezande, P.; Gevers, L. E. M.; Paul, J. S.; Vankelecom, I. F. J.; Jacobs, P. A. *J. Membr. Sci.* **2005**, *250*, 305–310.

(21) Prochazka, I. *Mater. Struct.* **2001**, *8*, 55–60.

(22) Hamada, Ch. He. E.; Suzuki, T.; Kobayashi, H.; Kondo, K.; Shantarovich, V. P.; Ito, Y. *J. Radioanal. Nucl. Chem.* **2003**, *255* (3), 431–435.

(23) Tao, S. J. *J. Chem. Phys.* **1972**, *56*, 5499.

(24) Eldrup, M.; Lightbody, D.; Sherwood, J. N. *Chem. Phys.* **1981**, *63*, 51.

(25) Baerdemaeker, J. De.; Dauwe, C. *Appl. Surf. Sci.* **2002**, *194*, 52.

(26) Hugenschmidt, C.; Dollinger, G.; Egger, W.; Lowe, B.; Mayer, J.; Pikart, P.; Piochacz, C.; Repper, R.; Schreckenbach, K.; Sperr, P. *Appl. Surf. Sci.* **2008**, *255*, 29–32.

(27) Kansy, J. *Nucl. Instrum. Methods Phys. Res., Sect. A* **1996**, *374* (2), 235–244.

(28) US Patent, 6 180 008, 2001.

(29) Gevers, L. E. M. The development and application of improved solvent-resistant nanofiltration membranes. Ph.D. Thesis, Katholieke Universiteit Leuven, 2005.

(30) US Patent, 6 180 008, 2001.

(31) Mulder, M. In *Basic Principles of Membrane Technology*, 2nd ed.; Mulder, M., Ed.; Kluwer Academic Publishers: Dordrecht, 2004; Chapter 3, pp 71−156.

(32) Vankelecom, I. F. J.; De Smet, K.; Gevers, L. E. M.; Jacobs, P. A. In *Nanofiltration. Principles and Applications*; Schäfer, A. I., Fane, A. G., White, T. D., Eds.; Elsevier: Oxford, 2005,; Chapter 3, pp 33−65.

JP9012653